2014 IEEE International Conference on Robotics & Automation (ICRA)
Hong Kong Convention and Exhibition Center
May 31 - June 7, 2014. Hong Kong, China

Optimization of the Workspace of a MEMS Hexapod Nanopositioner Using an Adaptive Genetic Algorithm

Hongliang Shi[1], Xuechao Duan[2] and Hai-Jun Su[3]

***Abstract*— This paper presents workspace optimization of a MEMS flexure-based hexapod nanopositioner previously built by the National Institute of Standards and Technology (NIST). Workspace is one of the most important quality criteria for positioning devices. Given a lot of literature on workspace optimization of rigid body parallel robots, there is relatively less work done in their compliant counterparts due to the challenges in determining the workspace. In this paper, we present an analytical formulation and a search algorithm to determine the workspace of the flexure based parallel mechanisms. A novel adaptive genetic algorithm has been developed to conduct the single and bi-objective optimization for maximum translational and rotational workspace. These optimization results provide a guidance for the designer to improve the device for specific design requirements.**

I. INTRODUCTION

A nanopositioner is a high precision positioning device used in motion control with a nanometer precision. Most nanopositioners are made of flexure mechanisms [1], [2] that are formed by multiple (often identical) flexure pivots, leaf springs or their chains that are designed to produce a defined motion upon the application of an appropriate load. These mechanisms have the advantage of no backlash and an ultra-high precision. Nanopositioners [3] have been widely used in precision engineering and play an important role in emerging nanotechnology and medicine [4].

The nanopositioner to be studied in this paper was built by the National Institute of Standards and Technology (NIST), shown in Figure 1. This hexapod nanopositioner has a parallel platform like mechanism for generating 6DOF motion by actuating three X-Y positioning stages with six thermal actuators [5].

Workspace is one of the most important quantitative measurements of nanopositioners. Much work has been done for the analysis and optimization of workspace of rigid body parallel robots [6]. Typically workspace can be classified into several types including constant orientation workspace or translational workspace, rotational workspace, dextrous workspace and so on. Shah et al. [7] applied CAD-enhanced workspace optimization to parallel manipulators. Tao and An [8] conducted workspace optimization for a 3-RRR parallel mechanism. Li and Xu [9] designed a 2DOF micromanipulator and optimized its workspace.

However, relatively few work has been done for workspace study for compliant mechanisms. Badescu and Constantinos [10] conducted a workspace optimization of a three-legged parallel platform with joint constraints. Xu and Li [11] did optimization of workspace and dexterity of a three-legged compliant micromanipulator.

In this work, we will study the workspace of the MEMS version of the hexapod nanopositioner. This workspace study is especially important since its workspace is very much limited by the parallel connection of three X-Y positioning stages as well as the elastic deformation of flexure joints.

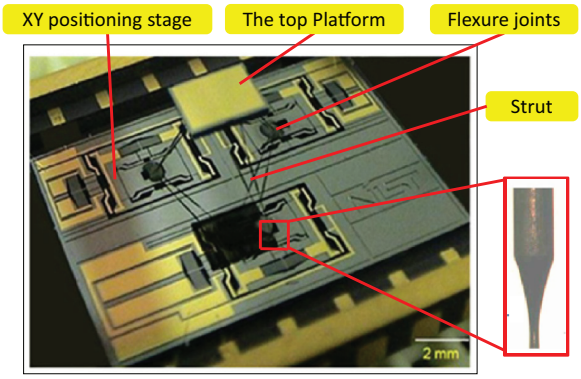

Fig. 1. The NIST hexapod nanopositioner.

II. GEOMETRIC DESCRIPTION OF THE POSITIONER

As shown in Fig. 1, the hexapod positioner studied in this paper is composed of three main parts: three X-Y positioning or actuation stages [5], six struts and one top platform. The top platform is the load-carrying part or the end-effector of the device. Three X-Y actuation stages, which can generate two orthogonal motions, are symmetrically laid out on the base plane. The moving plate of each X-Y stage supports two struts, which are firmly attached to the plate at one end $\mathbf{B}_i$ and to the top platform at the other end $\mathbf{A}_i$ both via the wire flexure joints as shown in Figure 2 (a).

The global coordinate system is placed at the home (undeformed) position of the geometrical center of the top platform. At the home position, the coordinates of the

*This material is based upon work supported by the National Science Foundation under Grant No: CMMI-1144022 and CMMI-1161841. Any opinions, findings, and conclusions or recommendations expressed in this material are those of the author(s) and do not necessarily reflect the views of the National Science Foundation.

[1]Research Associate in Department of Mechanical and Aerospace Engineering, The Ohio State University, Columbus, OH 43210, USA shi.347@osu.edu

[2]Associate professor in Institute on Mechatronics, Xidian University, Xi'an, 710071, China xchduan@xidian.edu.cn

[3]Assistant Professor in Department of Mechanical and Aerospace Engineering, The Ohio State University, Columbus, OH 43210, USA. Corresponding author. su.298@osu.edu

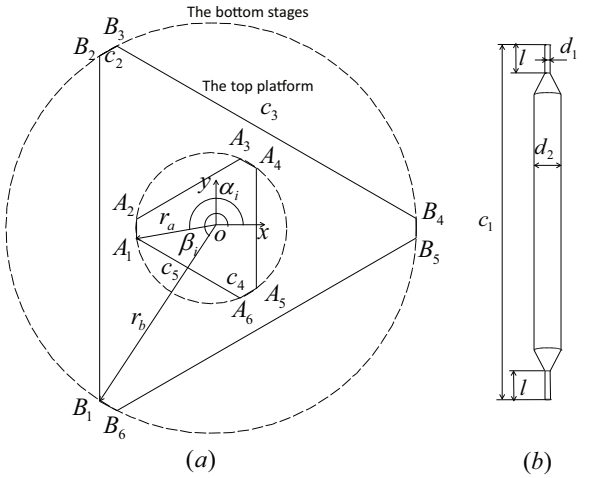

Fig. 2. Geometrical description of the hexapod mechanism. (a) the layout of the top platform and the bottom stages. (b) the supporting strut.

conjunction points are given by

$$\mathbf{A}_i^0 = [Z(\alpha_i)]\begin{Bmatrix} r_a \\ 0 \\ -t \end{Bmatrix}, \ \mathbf{B}_i^0 = [Z(\beta_i)]\begin{Bmatrix} r_b \\ 0 \\ -h \end{Bmatrix}, \ i = 1,\ldots,6 \quad (1)$$

where $[Z(\cdot)]$ is the 3 by 3 rotation matrix about the z axis, r_A and r_B are the radii of the strut attachment points (bottom plates in home position), h is the height of the hexapod mechanism, t is the thickness of the top platform. Angles α_i and β_i are tabulated in Table I.

As shown in Fig. 2 (b), the struts have a total length c_1 and diameter d_2, and have a short flexure joint of length l and diameter d_1 at each end ($d_1 \gg l$). The distance between the neighboring intersecting points of the struts at the top platform is c_4. The distance between the non-neighbor intersecting points of the struts at the top platform is c_5. For the base stages, the distance between the neighboring intersecting points of the struts is c_2. The distance between the non-neighboring intersecting points of the struts at the base is c_3.

The workspace of the hexapod nanopositioner is determined by the workspace of the X-Y actuation stages, maximum deformation angles of the twelve wire flexures and the layout of the six struts. In this work, we define $X = (c_1, c_2, c_3, c_4, c_5)^T$ as the design variables to be optimized while keeping all other geometric parameters constant. The dimensions of the current design are given in Table I. Our goal is to find an optimal set of these design parameters for a larger workspace of the top platform. In what follows, we discuss each part in details.

III. WORKSPACE OF ACTUATION STAGES

The X-Y actuation stage is composed of three main components: a thermal actuator, an amplifier mechanism and a guiding mechanism. As the thermal actuator can only produce force in one direction by increasing temperature, the workspace of the 2DOF X-Y positioning stage is a rectangle with S_x and S_y. In order to obtain the workspace of the X-Y

TABLE I

ORIGINAL GEOMETRIC DIMENSIONS OF THE HEXAPOD MECHANISM

l=0.08 mm, d_1=0.015 mm, d_2=0.075 mm, t=0.432 mm
h=4.127 mm, r_a=1.572 mm, r_b=4.277 mm
$\alpha_1 = 187.3^\circ, \alpha_2 = 172.7^\circ, \alpha_3 = 67.3^\circ, \alpha_4 = 52.7^\circ$
$\beta_1 = 237.3^\circ, \beta_2 = 122.7^\circ, \alpha_5 = -52.7^\circ, \alpha_6 = -67.3^\circ$
$\beta_3 = 117.3^\circ, \beta_4 = 2.7^\circ, \beta_5 = -2.7^\circ, \beta_6 = -117.3^\circ$
c_1=5.4 mm, c_2=0.4 mm, c_3=7.2 mm, c_4=0.4 mm, c_5=2.5 mm

positioning stage, we build the FE model in Abaqus. A set of concentrated forces is loaded on the thermal actuator and we record the displacement of the stage center and the Von Mises stress of the whole mechanism.

As shown in Fig. 3, when the von Mises stress reaches the yield stress with a safety factor of 3.5, we record the maximum displacement in x direction as $S_x = 59.69\mu m$. Similarly we obtain the value in y direction as $S_y = 59.94\mu m$.

$$0 \le \delta_x \le S_x, \quad 0 \le \delta_y \le S_y \quad (2)$$

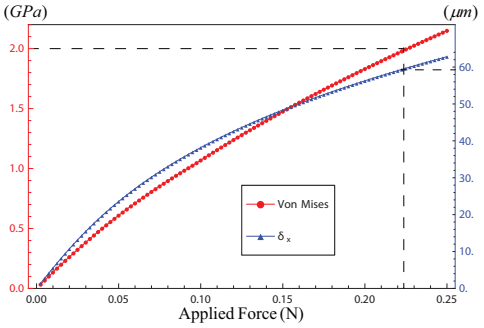

Fig. 3. The FE simulation result of the X actuation stage.

IV. WORKSPACE OF CIRCULAR WIRE FLEXURES

The wire flexures of the six struts all have a circular cross section of diameter d_1 and length of l. Since the length of struts is much larger, i.e. $c_1 \gg l$, the load to wire flexures is dominated by bending and torsional moment. To find the workspace of these wire flexures, we fix one end and apply an arbitrary bending moment M and torsion moment T to the other. The range of motion of the end planes is determined by the von Mises failure theory. See the details below.

The maximum normal and shear stresses occur on the outer fiber of the cross section. They are calculated as

$$\sigma_{max} = \frac{(d_1/2)M}{I} = \frac{(d_1/2)}{I}\frac{\psi EI}{l} = \psi\left(\frac{Ed_1}{2l}\right) \quad (3)$$

$$\tau_{max} = \frac{(d_1/2)T}{J} = \frac{(d_1/2)}{J}\frac{\phi GJ}{l} = \phi\left(\frac{Gd_1}{2l}\right) \quad (4)$$

where ψ and ϕ are the bending and torsion angles of the wire flexures respectively. $I = \pi d_1^4/64$ and $J = \pi d_1^4/32$ are the regular and polar moment of inertia of the cross section.

According to the von Mises failure theory, the wire flexure

will not fail when the following equation is satisfied

$$\sqrt{\sigma_{max}^2 + 3\tau_{max}^2} \leq \frac{\sigma_Y}{SF}, \tag{5}$$

where σ_Y is the material yield strength and SF is the safety factor. Substituting Eq.(3) and (4) into (5) yields

$$\psi^2 + 3\left(\frac{G}{E}\right)^2 \phi^2 \leq \left(\frac{2l}{Ed_1}\frac{\sigma_Y}{SF}\right)^2, \tag{6}$$

All wire flexures are made of tungsten material with a Young's modulus $E = 411GPa$, yield strength $\sigma_Y = 550MPa$, and poisson's ratio $\nu = 0.28$. Submitting these material properties, the geometrical parameters given in Table I and a safety factor $SF = 1.5$, we can derive the workspace of a wire flexure as

$$\psi^2 + 0.46\phi^2 \leq 1.98 \times 10^{-4} rad^2 \tag{7}$$

which represents an ellipse.

V. WORKSPACE OF THE HEXAPOD

A. Inverse kinematics

In the kinematic model of the positioner, the wire flexures are treated as spherical joints of which the centers are located at the intersection points of the flexures with the actuating stages and the top platform. When the device is at the home position, the coordinates of these joints are $\mathbf{A}_i^0$ and $\mathbf{B}_i^0$ given in (1). When the positioner is deformed, their new coordinates are denoted by $\mathbf{A}_i$ and $\mathbf{B}_i$ which are subject to the following kinematic constraint equations,

$$(\mathbf{A}_i - \mathbf{B}_i)^T(\mathbf{A}_i - \mathbf{B}_i) - c_1^2 = 0, \quad i = 1, \ldots, 6. \tag{8}$$

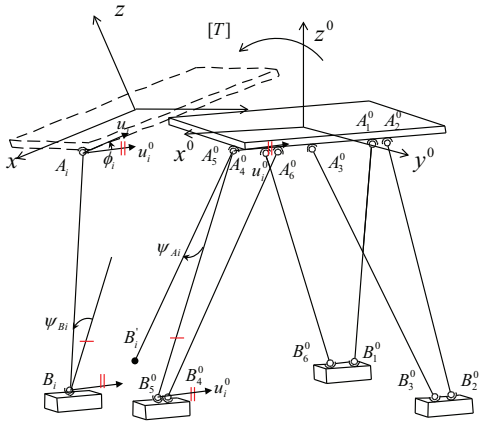

Fig. 4. The kinematic model of the positioner.

Substituting Eq. (1) and displacement of the X-Y actuation stages $\delta\mathbf{B}_i$ yields

$$([R]\mathbf{A}_i^0 + \mathbf{d} - \mathbf{B}_i^0 - \delta\mathbf{B}_i)^T([R]\mathbf{A}_i^0 + \mathbf{d} - \mathbf{B}_i^0 - \delta\mathbf{B}_i) - c_1^2 = 0, \tag{9}$$

where the 3 by 3 rotation matrix $[R]$ and vector $\mathbf{d}$ give the deformed orientation and position of the top platform relative to its home position. And $\delta\mathbf{B}_i$ are defined by:

$$\begin{aligned} \delta\mathbf{B}_1 = \delta\mathbf{B}_6 &= (\delta_{1x}, \delta_{1y}, 0)^T, \\ \delta\mathbf{B}_2 = \delta\mathbf{B}_3 &= (\delta_{2x}, \delta_{2y}, 0)^T, \\ \delta\mathbf{B}_4 = \delta\mathbf{B}_5 &= (\delta_{3x}, \delta_{3y}, 0)^T. \end{aligned} \tag{10}$$

To obtain six actuation $\delta\mathbf{B}_i$, we have to solve Eq.(9) which are mildly coupled quadratic equations. To find the bending angle ψ_{Ai}, ψ_{Bi} and torsion angle ϕ_{Ai}, ϕ_{Bi} of each individual flexure joint, we follow the derivation process of the NIST's MESO-scale hexapod nanopositioner presented in [12]. First, the bending angle ψ_i is defined as the angle between the undeflected limb $\mathbf{A}_i^0\mathbf{B}_i^0$ and deflected limb $\mathbf{A}_i\mathbf{B}_i$. Second, define two vectors $\mathbf{u}_i$, $\mathbf{v}_i$ which are attached on the moving platform and the bottom stages respectively. Third, calculate the deflected vectors $\mathbf{u}_i$, $\mathbf{v}_i$ and undeflected vectors $\mathbf{u}_i^0$, $\mathbf{v}_i^0$. And the torsion angle ϕ_i is determined by the change of the angle formed by vectors $\mathbf{u}_i$ and $\mathbf{v}_i$. See Fig. 4.

B. Kinematic constraints

For a given displacement $[R, \mathbf{d}]$ of the top platform, we determine whether or not it is within workspace by checking if both the actuation displacements and wire flexures are within their workspaces. More specifically, we use the following steps.

1) Calculate the actuation of three X-Y positioning stages, δ_{1x}, δ_{1y}, δ_{2x}, δ_{2y}, δ_{3x}, δ_{3y}, and check if they satisfy the constraints (2), i.e.

$$\begin{aligned} &0 \leq \delta_{1x} \leq S_x, \quad 0 \leq \delta_{1y} \leq S_y, \quad 0 \leq \delta_{2x} \leq S_x \\ &-S_y \leq \delta_{2y} \leq 0, \quad -S_x \leq \delta_{3x} \leq 0, \quad -S_y \leq \delta_{3y} \leq 0 \end{aligned} \tag{11}$$

where the negative signs are due to the layout of the three X-Y actuation stages.

2) Calculate the bending angle ψ_{Ai}, ψ_{Bi} and torsion angle ϕ_{Ai}, ϕ_{Bi} of each flexure joint and check if they satisfy the constraints (7), i.e.

$$\begin{aligned} &\psi_{Ai}^2 + 0.46\phi_{Ai}^2 \leq 1.98 \times 10^{-4} rad^2, \quad i = 1, \ldots, 6 \\ &\psi_{Bi}^2 + 0.46\phi_{Bi}^2 \leq 1.98 \times 10^{-4} rad^2, \quad i = 1, \ldots, 6 \end{aligned} \tag{12}$$

Essentially, the 6DOF workspace of the hexapod is limited by the above eighteen constraint functions (11-12).

C. Workspace determination

We first denote the three dimensional translational and rotational workspace by Δ and Θ respectively. Here Δ is defined as the volume enclosed by the boundaries of the top platform displacement $(\delta_x, \delta_y, \delta_z)$ with a fixed zero rotation. Let us denote the gravity center of the workspace volume by P_c. And the rotational workspace Θ is defined as the volume enclosed by the boundaries of three angles $(\theta_x, \theta_y, \theta_z)$ when the position of the platform is fixed at the gravity center P_c.

To determine the volume of the workspace, the workspace is first sliced into a series of subspace by a series of equally spaced planes parallel to XY plane. We then develop a rapid polar searching algorithm (RPSA) to determine planar area of the subspace and calculate the accumulated volume to obtain

the whole workspace volume. The process for determining Δ is detailed described as follows.

1) Start searching at the polar coordinate center towards polar axis. Increase ρ with step size δ_ρ and check whether the position meets constraint functions (11-12). Until the point does not meet at least one of the constraints, we denote the point as out of boundary condition so that the previous point A_0 is denoted as the workspace boundary point on the polar axis. And we denote the radius and the position of A_0 as ρ_0 and $A_0(\rho_0, 0)$. See Fig.5(a).
2) Increase polar angle with a step size δ_γ with the same polar radius, so that we obtain the test point $T_1(\rho_0, \delta_\gamma)$.
3) Check whether any of the constraints takes effect at the position of T_1. If none of the constraints takes effect, it indicates that T_1 is still within the workspace. Therefore, we increase ρ_0 with δ_ρ until one of the constraint functions is not satisfied. Thus, we can find the second boundary point $A_1(\rho_1, \delta_\gamma)$.
4) Decrease the radius with $\delta\rho$, if the test point T_2 is out of the workspace. Until the position meets all the constraint functions, we can obtain $A_2(\rho_2, 2\delta_\gamma)$ as the boundary point.
5) Conduct the searching so forth and finish the process when $\gamma = 2\pi$. The searching area is calculated as

$$A = \frac{1}{2}\sum_{i=1}^{m} \rho_i^2 \delta_\gamma. \tag{13}$$

where m is defined as $2\pi/\delta_\gamma$. The steps 1-5 are defined as the process of RPSA.
6) Define the base plane at $z = z_0$. Here, we choose $z_0 = 20\mu m$ for Δ and $z_0 = 0$ for Θ. Choose n points and define them as the candidate start points of workspace searching. Do RPSA at the candidate points. Pick out the robust (with maximum section area) and the related candidate is denoted as the start point C_0. Calculate the geometrical center of the area as P_1
7) Search the workspace upward and downward from the base plane respectively with a step size δ_z. Treat P_1 as the new polar coordinate center for RPSA.
8) Continue the searching by updating the geometrical center P_n of the previous layer as the new polar frame center of the current layer. Until the layer area equals to zero, the searching reaches the terminating condition. The workspace volume is derived as

$$\Delta = \sum_{i=1}^{n} A_i \delta_z. \tag{14}$$

where n is the number of the layers.

Similarly we can determine the rotational workspace Θ.

VI. OPTIMIZATION USING ADAPTIVE GENETIC ALGORITHM

Genetic algorithm (GA) optimizers are stochastic optimization techniques based on the concepts of natural selection, which are especially effective for the combinatorial optimization problems as in this research [13].

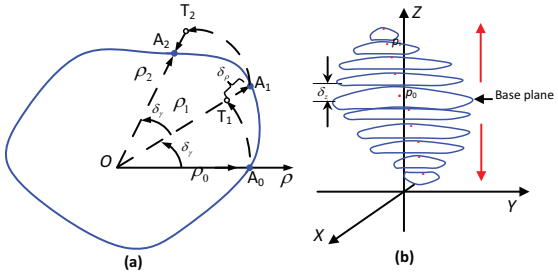

Fig. 5. Schematic of workspace slices and rapid polar searching algorithm(RPSA)

A. Real-coded scheme and fitness function

Generally, there are two dominate coding schemes for GAs: binary and real coding schemes[14]. For sake of obtaining the shorter length of genetic code and making the genetic operations easier, the real coding is preferred in problems with a great number of variables [15]. The candidate solutions of the optimization problem are encoded into the real number genes of the chromosome directly.

Besides, in order to enhance the sensitivity of the fitness function concerning the design parameter, the workspace function is constructed as follows

$$F(X) = k_0 \Omega_i(X), i = 1, 2, 3. \tag{15}$$

where $k_0 > 1$ and i indicates different type of workspace volume.

B. Genetic operations

These following three operations are particularly designed for the real-coded GA.

The tournament selection operator is used here in order to avoid the premature phenomenon. In which two candidate solutions are chosen from the population and just the one with higher fitness is copied to the new population each time, which is repeated until the new temporary population is formed.

Crossover is the course in which certain pairs of chromosomes are chosen according to the preset crossover probability from the newly-born population mentioned according to the following arithmetical crossover operator [15], [16]

$$X_1' = \lambda X_1 + (1-\lambda)X_2, \quad X_2' = \lambda X_2 + (1-\lambda)X_1 \tag{16}$$

where X_1 and X_2 are the two parents to be implemented the crossover operation while X_1' and X_2' are the offspring after crossover operation, crossover factor λ is a preset-constant belonging to interval $(0, 1)$.

Mutation involves the modification of the value of gene in certain chromosomes chosen from the population. For a given parent X, the stochastic number τ generated with even probability in $\{0, 1\}$ determines the way to generate the offspring chromosome

$$X_i' = \begin{cases} X_i + \Delta(t, \overline{X}_i - X_i), \tau = 0 \\ X_i - \Delta(t, X_i - \underline{X}_i), \tau = 1 \end{cases} \tag{17}$$

where function $\Delta(t,y) = y\varsigma(1-t/N)^k$, ς is a random number with the range of $[0,1]$, t is the current generation, N is the maximum generation of the genetic evolution, and k is a preset parameter determining the degree of nonuiformity. $\overline{X}_i$ and $\underline{X}_i$ indicate the upper and lower boundaries of X_i, the ith component of X separately, where $i = 1,2,...,M$. M is the population size.

C. Adaptation of crossover and mutation probability

The crossover probability P_c and mutation probability P_m decides how many chromosomes will be chosen to take part in the crossover and mutation, respectively. If P_c and P_m are set a constant number either too small or too large, it will lead to the premature of the GAs, i.e. the optimization result will be trapped in local optima.

By extending methodology of adaptive probability of crossover and mutation proposed by Srinivas [17], the following function is used to give the adaptive P_c and P_m,

$$P_c = \frac{1+e^{-s}}{2}P_{c0}, \quad P_m = \frac{1+e^{-s}}{2}P_{m0} \tag{18}$$

where $s = \sqrt{\frac{1}{M}\sum_{i=1}^{M}[F(\mathbf{X}(i)) - \bar{F}]^2}$, and $\bar{F}$ is the average fitness of the ith generation population. P_{c0} and P_{m0} are the initial value of the crossover and mutation probability respectively.

Herein, at the initial stage, the random generated initial population decides a large value of s of the algorithm, and then a small crossover and mutation probability result in relatively few chromosomes picked out to implement crossover and mutation, which will preserve the elite chromosomes farthest. In the ending generations, the fitness of the chromosomes becomes concentrated, thus decreasing the value of s and increasing P_c and P_m, and more chromosomes will participate the crossover and mutation operations. Consequently, the diversity of the population is maintained from beginning to end as the adaptive GA proceeds and the global optima is obtained.

The elitist preserving strategy is also adopted in the algorithm to guarantee no decrease in fitness from one generation to the next. The maximum evolution generation is selected as the termination criterion of the adaptive GAs.

VII. OPTIMIZATION RESULTS AND ANALYSIS

In this section, we apply the proposed adaptive GA to optimize the workspace of the hexapod positioner.

A. Define the optimization problems

Design optimization parameter is donated as $X = (c_1, c_2, c_3, c_4, c_5)^{\mathrm{T}}$ which are illustrated in Fig.2. The original values, upper and lower boundaries conditions of design parameters are shown in Table II.

The objective function for GA optimization is based on the volume Δ and Θ obtained with our search algorithm RPSA presented earlier. For the optimization of the rotational workspace and translational workspace, the objective function are defined as

$$F_\Theta(X) = \Theta, \quad F_\Delta(X) = \Delta/V \tag{19}$$

where $V = \pi r_b^2 h$ is the packaging volume of the device. r_b is the radius of the circle in the base plane and h is the height of the top platform, calculated by Eq. (9). Essentially we would like to maximize the translational workspace per unit packaging volume.

TABLE II
VARIABLES AND PARAMETERS OF THE OBJECTIVE FUNCTION

X	$c_1(\mu m)$	$c_2(\mu m)$	$c_3(\mu m)$	$c_4(\mu m)$	$c_5(\mu m)$
X_0	5400	400	7200	400	2500
$\overline{X}$	7000	465	9333	600	2530
$\underline{X}$	4000	180	5500	180	600
$generation = 100,\ M = 60,\ \lambda = 0.5,$					
$P_{c0} = 0.8,\ P_{m0} = 0.8,\ k_0 = 10^3$					

B. Single objective optimization

The computation parameter of the AGA is listed in Table.II. After 100 iterations, optimal solutions $X_1^* = (5257.85, 307.50, 5561.01, 222.31, 728.42)^{\mathrm{T}}$ and $X_2^* = (6302.9, 183.5, 5603.6, 205.4, 1581.6)^{\mathrm{T}}$ for translational and rotational workspace are obtained. With the 12 cores parallel computation, the running time for translational workspace optimization can be reduced form $671.40s$ to $44.77s$ on a Intel Xeon(R) CPU E7-4870 and Windows Server 8 system.

For the single objective optimization, we start at initial solution X_0 in Table II. The translational and rotational workspace values for the initial and optimal solution is list in Table III. The values of original and optimal Δ are very close, and are also shown in Fig. 6 (a). However, the packaging volume V is much smaller for the optimal solution. Thus, $F_\Delta(X)$ is optimized 46%. Furthermore, $F_\Theta(X)$ is optimized 72% and it is shown in Fig. 6 (b).

TABLE III
RESULT OF SINGLE OBJECTIVE OPTIMIZATION

Type	Initial function	Optimal function	Improved
Δ	2.27×10^4	2.07×10^4	
V	2.62×10^{11}	1.64×10^{11}	
$F_\Delta(X)$	8.65×10^{-8}	1.26×10^{-7}	46%
$F_\Theta(X)$	0.0445	0.0767	72%

C. Bi-objective optimization

For many applications, both translational and rotational workspace are important. It makes sense that the following weighted sum model of the bi-objective optimization is used as the objective function,

$$F_{\Delta\Theta}(X) = \alpha \frac{2F_\Delta(X)}{F_\Delta(X)+\max(F_\Delta)} + \beta \frac{2F_\Theta(X)}{F_\Theta(X)+\max(F_\Theta)} \tag{20}$$

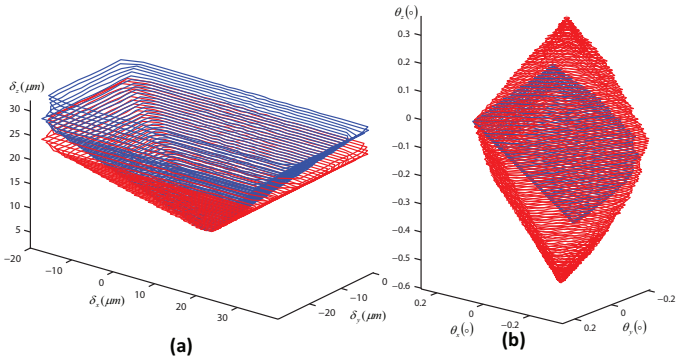

Fig. 6. The initial (blue) vs. the optimal (red) workspace. (a) Translational workspace (b) Rotational workspace

where $\alpha, \beta \in [0,1]$ and $\alpha + \beta = 1$. $\max(F_\Delta)$ and $\max(F_\Theta)$ are respectively the maximum values of the translational and rotational workspace given in Table III, which are obtained by the single objective optimization.

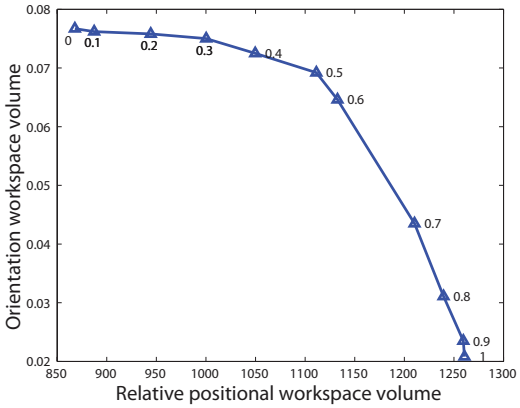

Fig. 7. Pareto front of the bi-objective optimization

The Pareto front is illustrated in Fig.7. The triangular marks indicate the different optima obtained with different coefficients. The figures near each mark shows its involved value of coefficient α in the weighted sum model mentioned above. The Pareto front shows the dependence of the bi-objective functions on the coefficients, which is the measure of the designers' preference. Under the condition that one of the two objectives is preferred to maximal extent for instance $\alpha = 0$ or $\alpha = 1$, the bi-objective optimization degenerates into a single objective optimization.

VIII. Conclusion

In this paper, we present a method for calculating the workspace of the NIST's MEMS hexapod nanopositioner, which is based on the limits of the flexure joints and the workspace of the X-Y positioning stages. This method can be applied to the workspace derivation of general parallel platform mechanisms with flexure joints. A rapid polar searching algorithm has been developed to quantify the volume of workspace. By adapting crossover and mutation probability, a novel adaptive genetic algorithm has been developed. As a result of the single objective optimization, the translational and rotational workspace has been improved by 46% and 72% respectively. Finally, we conducted a bi-objective optimization based on the designer's preference. These results serve an important guidance for next generation design of this device. In the future work, a stiffness model with loading and dynamic studies could be derived for specific application of the hexapod nanopositioner. Besides, Finite Element simulation could be did for validation of the workspace derivation.

References

[1] H. Soemers, *Design Principles for Precision Mechanisms*. Enschede: T-Pointprint, 2010.

[2] H.-J. Su, H. Shi, and J. Yu, "A symbolic formulation for analytical compliance analysis and synthesis of flexure mechanisms," *ASME Journal of Mechanical Design*, vol. 134, no. 5, p. 051009, 2012.

[3] H. Shi, H.-J. Su, N. Dagalakis, and J. A. Kramar, "Kinematic modeling and calibration of a flexure based hexapod nanopositioner," *Precision Engineering*, vol. 37, no. 1, pp. 117 – 128, 2013.

[4] Q. Liang, D. Zhang, Q. Song, and Y. Ge, "Micromanipulator with integrated force sensor based on compliant parallel mechanism," in *2010 IEEE International Conference on Robotics and Biomimetics (ROBIO)*. IEEE, Dec. 2010, pp. 709–714.

[5] Y.-S. Kim, J.-M. Yoo, S. H. Yang, Y.-M. Choi, N. G. Dagalakis, and S. K. Gupta, "Design, fabrication and testing of a serial kinematic MEMS XY stage for multifinger manipulation," *Journal of Micromechanics and Microengineering*, vol. 22, no. 8, p. 085029, 2012.

[6] J. Merlet, *Parallel Robots*, 2nd ed. Springer, Feb. 2006.

[7] H. Shah, M. Narayanan, and V. Krovi, "CAD-enhanced workspace optimization for parallel manipulators: A case study," in *2010 IEEE Conference on Automation Science and Engineering (CASE)*, 2010, pp. 816–821.

[8] Z. Tao and Q. An, "Interference analysis and workspace optimization of 3-RRR spherical parallel mechanism," *Mechanism and Machine Theory*, vol. 69, pp. 62–72, Nov. 2013.

[9] Y. Li and Q. Xu, "A novel design and analysis of a 2-DOF compliant parallel micromanipulator for nanomanipulation," *IEEE Transactions on Automation Science and Engineering*, vol. 3, no. 3, pp. 247–254, 2006.

[10] M. Badescu and C. Mavroidis, "Workspace optimization of 3-legged UPU and UPS parallel platforms with joint constraints," *Journal of Mechanical Design*, vol. 126, no. 2, pp. 291–300, May 2004.

[11] Q. Xu and Y. Li, "Kinematic analysis and optimization of a new compliant parallel micromanipulator," *International Journal of Advanced Robotic Systems*, vol. 3, no. 4, 2006.

[12] H. Shi and H.-J. Su, "An analytical model for calculating the workspace of a flexure hexapod nanopositioner," *ASME Journal of Mechanisms and Robotics*, vol. 5, no. 4, p. 041009, 2013.

[13] R. L. Haupt, "An introduction to genetic algorithms for electromagnetics," *IEEE Antennas and Propagation Magazine*, vol. 37, no. 2, pp. 7–15, 1995.

[14] C. H. Dai, Y. Zhu, and W. Chen, "Adaptive probabilities of crossover and mutation in genetic algorithms based on cloud model," in *Proceeding of IEEE Information Theory Workshop. ITW '06 Chengdu*, 2006, pp. 710–713.

[15] H. Abbas and M. Bayoumi, "Volterra-system identification using adaptive real-coded genetic algorithm," *IEEE Transactions on Systems, Man and Cybernetics, Part A: Systems and Humans*, vol. 36, no. 4, pp. 671–684, 2006.

[16] R. Esmaelzadeh, "Rendezvous trajectory optimization using real genetic algorithm combined with gradient method," *WSEAS Transactions on Systems*, vol. 5, no. 12, pp. 2875–2880, 2006.

[17] M. Srinivas and L. Patnaik, "Adaptive probabilities of crossover and mutation in genetic algorithms," *IEEE Transactions on Systems, Man and Cybernetics*, vol. 24, no. 4, pp. 656–667, 1994.